17th World Conference on Earthquake Engineering, 17WCEE
Sendai, Japan - September 27th to October 2nd, 2021

FEASIBILITY STUDY ON REDUCING DAMAGE TO RC COLUMN WITH WING WALLS BY REMOVING WALL VERTICAL REBAR ANCHORAGE

Z. Zhang(1), Y. Sanada(2), R. Yoon(3), K. Kusunoki(4), Y. Hibino(5), T. Mukai(6)

(1) *Ph.D. Candidate, Osaka University, Osaka, Japan, zhang_zheng@arch.eng.osaka-u.ac.jp*
(2) *Professor, Osaka University, Osaka, Japan, sanada@arch.eng.osaka-u.ac.jp*
(3) *Assistant Professor, Osaka University, Osaka, Japan, Yoon_rokhyun@arch.eng.osaka-u.ac.jp*
(4) *Professor, The University of Tokyo, Tokyo, Japan, kusunoki@eri.u-tokyo.ac.jp*
(5) *Associate Professor, Nagoya University, Nagoya, Japan, hibino@nuac.nagoya-u.ac.jp*
(6) *Senior Research Engineer, Building Research Institute, Tsukuba, Japan, t_mukai@kenken.go.jp*

Abstract

The field investigation performed during the latest earthquakes such as the 2011 off the Pacific coast of Tohoku earthquake and 2016 Kumamoto earthquake revealed that reinforced concrete (RC) buildings that satisfied the standards for earthquake resistant design survived. However, the non-structural walls such as wing, hanging/spandrel walls suffered severe damage which resulted in restoration and demolition of damaged buildings. This study proposes a new rebar arrangement of wing walls which removes the wall vertical rebar anchorage to reduce earthquake damage. The major objectives are to study the effects of the removal of wall vertical rebar anchorage on the seismic performance of a prototype column with wing walls on both sides, such as strength, ductility, and damage process. Cyclic loading tests were carried out using two 1/2 scale RC column specimens with wing walls. The difference between the two specimens was the presence/absence of wall vertical rebar anchorage. The experimental results showed that the removal of wall vertical rebar anchorage reduced damage on the wing walls and increased the ductility performance, while the strength was a little decreased because of the removal. Moreover, a quantitative seismic damage evaluation in terms of crack width and length was carried out to investigate the correlation between the seismic damage and the limit states. Furthermore, the experimental performance such as the ultimate flexural strength and deformation capacity was simulated by conventional bending analysis. The analytical results generally showed good agreements with the experimental results; thus, the bending analysis scheme presented in this study was effective for simulating the seismic performance of the column with the wing walls removing the vertical rebar anchorage proposed in this study.

Keywords: Anchorage; Bending analysis; Column with wing walls; Damage control; Seismic performance.

1. Introduction

Based on the investigation of the 2011 off the Pacific coast of Tohoku earthquake and 2016 Kumamoto earthquake [1, 2], reinforced concrete (RC) buildings that satisfied the standards for earthquake resistant design launched in 1981 in Japan (hereafter, current Japanese standards) survived, while many of those buildings could not be continually occupied after the earthquakes due to severe damage to columns with wing walls with high stiffness. The current Japanese standards require two levels of design criteria: (i) no damage or repairable under moderate earthquakes and (ii) no collapse and saving human lives under severe earthquakes. In other words, the second criterion accepts scenarios where buildings may lose their functions due to severe damage. However, regardless of such minimum requirements in the current Japanese standards, social demand for the seismic performance of buildings has been changed, namely, continuity of building functions after large earthquakes is getting more and more important. Thus, to maintain the continuity of building functions after such earthquakes, it is essential to reduce damage not only to structural components but also to non-structural ones.

In this study, a new rebar arrangement of wing walls that removes the wall vertical rebar anchorage is proposed to reduce damage to RC columns with wing walls, as shown in Fig. 1. The present paper describes a series of experiments with two specimens which included one standard RC column with wing walls (with the wall vertical rebar anchorage) and the other RC column with wing walls without that. The major objectives were to study the effects of the removal of wall vertical rebar anchorage on their seismic performance such as strength, ductility, and damage progress. Damage in terms of crack width and length was investigated at different drift levels to observe the damage progress of both RC columns with wing walls. The damage level was assessed based on the 2004 AIJ guidelines [3] to study the validity of removing the wall vertical rebar anchorage. Then, the experimental performance of the specimens such as the ultimate flexural strength and deformation capacity was evaluated utilizing conventional bending analysis to investigate the applicability to the columns with wing walls removing the vertical rebar anchorage. Findings from the above experimental and numerical studies contribute to approach future RC buildings to realize the continuity of building functions even after severe earthquakes.

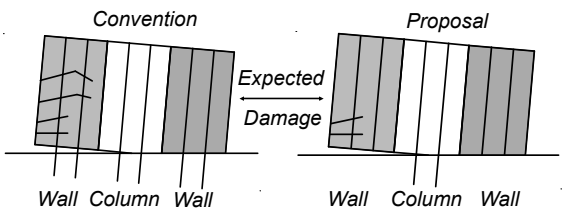

Fig.1 Proposal

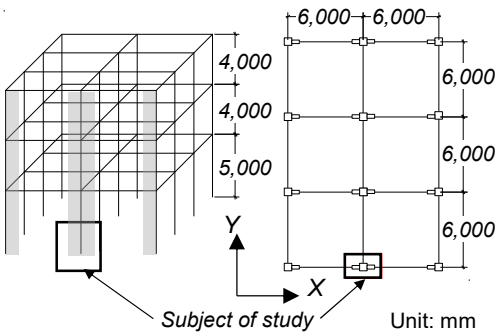

Fig. 2 Configurations and plan of the prototype building

2. Experimental program

2.1 Specimens description and materials

Fig. 2 shows a prototype RC building which consists of two spans in the X direction and three spans in the Y direction and has three layers (5 m on the ground floor, 4 m on the 2nd and 3rd floors). A static cyclic loading test was planned, using two 1/2 scale columns with wing walls designed to represent the first-story center column with wing walls (boxed in Fig. 2), as summarized in Table 1. Fig. 3 shows the reinforcement arrangements of the specimens. Fig. 4 shows the cross-sectional details of the specimens. All specimens were satisfied the requirements for semi-ductile design based on the standards of Architectural Institute of Japan (hereinafter, AIJ standards) [4] (semi-ductile design and confining rebar ratio less than 0.6%), as shown in Table 2. The specimen CW-JPL represented a conventional column with wing walls with the wall vertical

Table 1 Structural details of the specimens

			CW-JPL	CWN-JPL
Column	b × D (mm)		250 × 250	
	Longitudinal rebar		10-D16 (p_g=3.18%)	
	Horizontal rebar		D6@50 (p_w=0.51%)	
	Concrete cover (mm)		25	
Wing walls	Horizontal rebar		2-D6@100 (p_s=0.51%)	
	Vertical wall rebar		2-D6@100	
	Length of confined area (mm)		130	
	Confining rebar		D6@100	
	Confining rebar ratio (%)	X direction	1.01	
		Y direction	0.39	0.41
	Concrete cover (mm)		20	
Concrete design strength (N/mm^2)			36	
Ultimate flexural strength (kN)			156.7	140.8
Ultimate shear strength (kN)			209.2	
Shear margin			1.33	1.49

p_g: Gross longitudinal reinforcement ratio of column
p_w／p_s: Horizontal reinforcement ratio of column／wall

Table 2 Member classificaiton of the column with wing walls for the AIJ standard [4]

	Ductile design	Semi-ductile design	(Semi-ductile design)	
			CW- JPL	CWN-JPL
Q_{su} / Q_{mu}	Greater than/equal to 1.25	Greater than/equal to 1.1	1.33	1.49
h_0 / D	Greater than/equal to 2.5	Greater than/equal to 2.0	6.4	
σ_0 / F_c	Less than/equal to 0.35	Less than/equal to 0.45	0.072	
$(p_g\sigma_y+\sigma_{0w})$ / F_c	Less than/equal to 1/3	Less than/equal to 1/2	0.41	
t_w / $\sqrt{A_c}$	Greater than/equal to 4/10	Greater than/equal to 3/10	0.5	
τ_u /F_c	Less than/equal to 0.1	Less than/equal to 0.125	0.046	

※Satisfying greater than/equal to 0.6% in 2/3 of the compressive zone as well as the requirements for semi-ductile design, it can be replaced by ductile design.
Q_{su}/Q_{mu}: shear margin, h_0: column inner height, D: column width, σ_0, σ_{0w}: axial force ratio for column, F_c: concrete design strength, p_g: longitudinal rebar ratio, σ_y: longitudinal rebar yield stress, t_w: wall thickness, A_c: cross-sectional area of column, τ_u: shear stress ratio for cross section (including wall)

Table 3 Material properties of concrete

	CW-JPL	CWN-JPL
Elastic modulus	31.0 kN/mm^2	30.3 kN/mm^2
Compressive strength	48.1 N/mm^2	52.8 N/mm^2
Strain at compressive strength	2458μ	2774μ

Table 4 Material properties of reinforcement

(SD345)	D6	D16
Elastic modulus	185kN/mm^2	196kN/mm^2
Yield stress	403 N/mm^2	389 N/mm^2
Strain at yield stress	2187μ	1982μ
Tensile strength	598 N/mm^2	574 N/mm^2

rebar anchorage. The new wall vertical rebar arrangement proposed in Fig. 1 was applied to the specimen CWN-JPL. The experimental parameter was the presence/absence of wall vertical rebar anchorage. The structural details of the specimens CW-JP and CWN-JPL were common except for the removal of the wall vertical rebar anchorage at the bottoms of the wing walls for CWN-JPL. The wall confining rebar had a 135- and 90-degree hook at one end and at the other end, as shown in Fig. 5. D6@100 U-shaped horizontal rebar

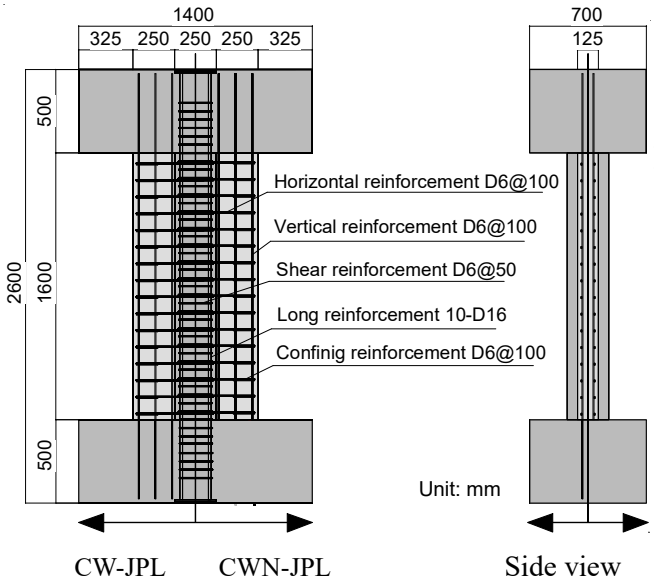

Fig. 3 Reinforcement arrangement of the specimens

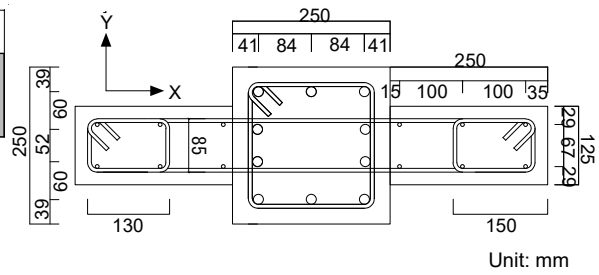

Fig. 4 Cross-sectional details of the specimens

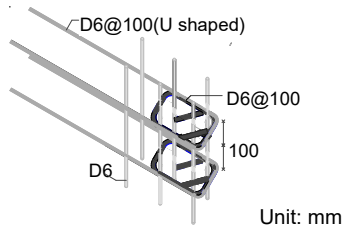

Fig. 5 Close-up of confined area

was used to connect the wing walls and column. Ultimate flexural and shear strengths shown in Table 1 were calculated based on the ACI stress block method [5] and Eq. 1 [4], respectively.

$$Q_{su} = \left\{ \frac{0.053 p_t^{0.23}(F_c + 18)}{M/(Qd_e) + 0.12} + 0.85\sqrt{p_{we}\sigma_{wh}} + 0.1\sigma_0 \right\} b_e j_e + 0.1N$$

$$p_{we} = p_w \left(b/b_e \right) + p_s \left(t/b_e \right) \tag{1}$$

where p_t: tensile longitudinal rebar ratio (%), b: column width, F_c: compression strength of concrete, $M/(Qd_e)$: shear span ratio, d_e: effective depth (distance between the center of tensile rebar and exterior edge of compression zone), p_w: shear rebar ratio of the column, b: column width, b_e: width of a rectangular replacement section, t: wall thickness, p_s: horizontal rebar ratio of the wall, σ_{wh}: yield stress of the shear rebar, j_e: stress center distance, and N: axial force.

In addition, the cylindrical compressive strength of the concrete and the properties of the reinforcement are shown in Tables 3 and 4, respectively.

2.2 Experimental methods

A test setup in the loading system is shown in Fig. 6. The specimens were mounted onto the fixed base by using PC steel bars in the loading system which consisted of one horizontal (1,000kN) and two vertical hydraulic jacks (2,000kN), as shown in Fig.6. Every specimen was subjected to a constant axial load of N/N_0=0.072 (where N is the axial load, and N_0 is the compressive strength of the column). Equation 1 gives axial forces to maintain in the south (N_S) and north (N_N) vertical jacks during the experiment to obtain the bending moment diagram as shown in Fig. 6.

$$N_s = \frac{N}{2} + \frac{Q}{L}a$$
$$N_n = \frac{N}{2} - \frac{Q}{L}a \tag{2}$$

where N_S and N_N are axial forces in the south and north vertical jacks (kN); N is total axial load on the specimen (kN); Q is lateral force (kN); L is center to center distance between the south and north vertical jacks (= 4,000

Table 5 Loading histories

Drift (% rad)	CW-JPL	CWN-JPL
Short-term allowable shear force	1 cycle	1 cycle
0.25	2 cycles	2 cycles
0.33		
0.5		
0.66		
1.0		
1.33		
2.0		
2.66		
4.0	-	

Table 6 Short-term shear force (AIJ Standard [6])

Specimen	CW-JPL	CWN-JPL
Short-term allowable shear force	66.6 kN	59.0 kN
Material under the allowable stress	Raber (wall)	Concrete

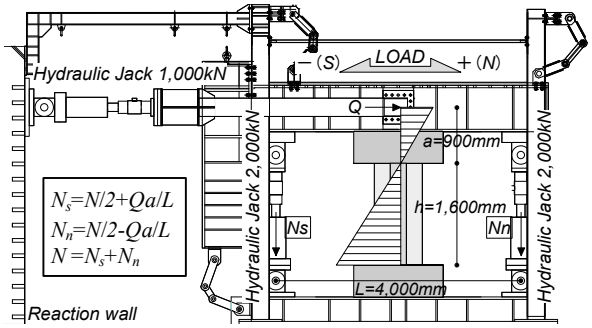

Fig. 6 Loading system

mm) and a is distance between the assumed inflection height and the center of loading beam (=900 mm), as shown in Fig. 6.

The lateral loading was controlled by a drift angle R (rad) which was a ratio of lateral displacement to the specimen clear height of 1,600 mm. The loading protocol had an initial cycle of R at the short-term allowable shear force (when concrete and/or longitudinal rebar reached the short-term allowable stress at the bottom of each specimen [6] followed by the cycles to R = 0.25%, 0.33%, 0.5%, 0.66%, 1.0%, 1.33%, 2.0%, 2.66% and 4.0% rad. One cycle was applied until the strain of column longitudinal rebar exceeded 50% of the yield strain, and two cycles were applied thereafter, as shown in Table 5. Table 6 shows the calculation results of the short-term allowable shear force.

3. Experimental results

3.1 Shear force–drift angle relationships and damage progress

Fig. 7 shows the shear force–drift angle relationships of both specimens. Fig. 8 compares crack patterns of the specimens during the tests. Solid and dotted lines show cracks observed in the positive and negative loadings, respectively.

[Specimen CW-JPL with the wall vertical rebar anchorage]
Flexural cracks were observed at the bottom of wing walls and column at the cycle to the short-term allowable shear force. More flexural cracks were observed from the bottom to mid-height of the wing walls and column from the cycle of R = 0.25% rad. Tensile yielding of the vertical rebar in wing walls occurred at R = 0.2% rad and R = -0.16% rad. Then, the existing/new flexural cracks extended with increasing of the drift as the wall vertical rebar was anchored into the base stub. The column main rebar yielded at the cycle to R = 0.5% rad. The maximum strengths of 197.2 kN and -199.8 kN were observed during the cycle of R = ±1.0 % rad. The lateral load decreased with damage to the wall confined area showing concrete crush at the bottom of the wing wall in a height approximately 2.5 times the wall thickness (shown as Fig. 8(a)) in the following cycle. During the cycle of R = 2.0% rad, buckling of the vertical rebar in the wing walls was observed. The lateral load decreased to 80% of the maximum strength at R = -2.55% rad; thus, the loading was completed at the cycle of R = 2.66% rad.

[Specimen CWN-JPL without the wall vertical rebar anchorage]
Similar to CW-JPL, flexural cracks were observed at the bottom of wing walls and column at the cycle to R of the short-term allowable shear force, while few new flexural cracks occurred from the bottom to mid-height at

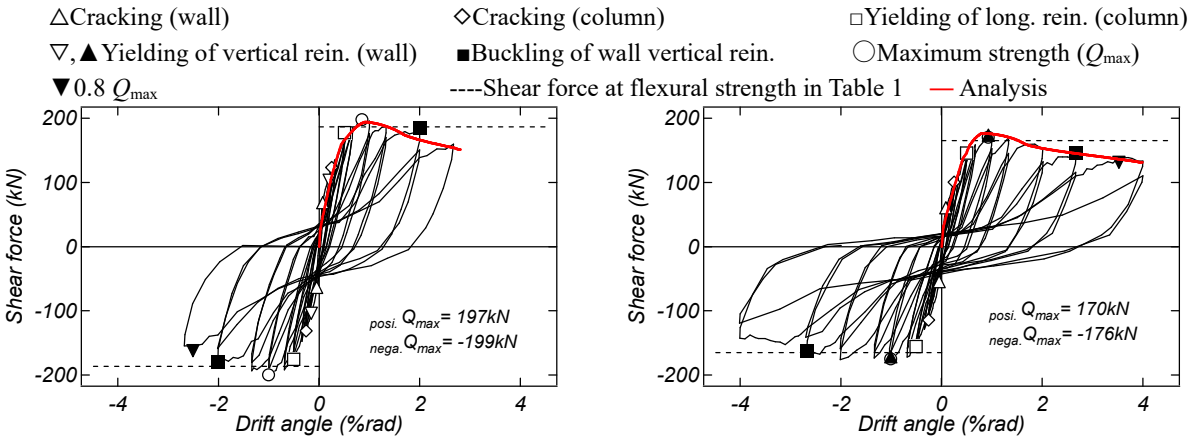

(a) CW-JPL (with the anchorage) (b) CWN-JPL (without the anchorage)

Fig.7 Shear force vs. drift angle relationships

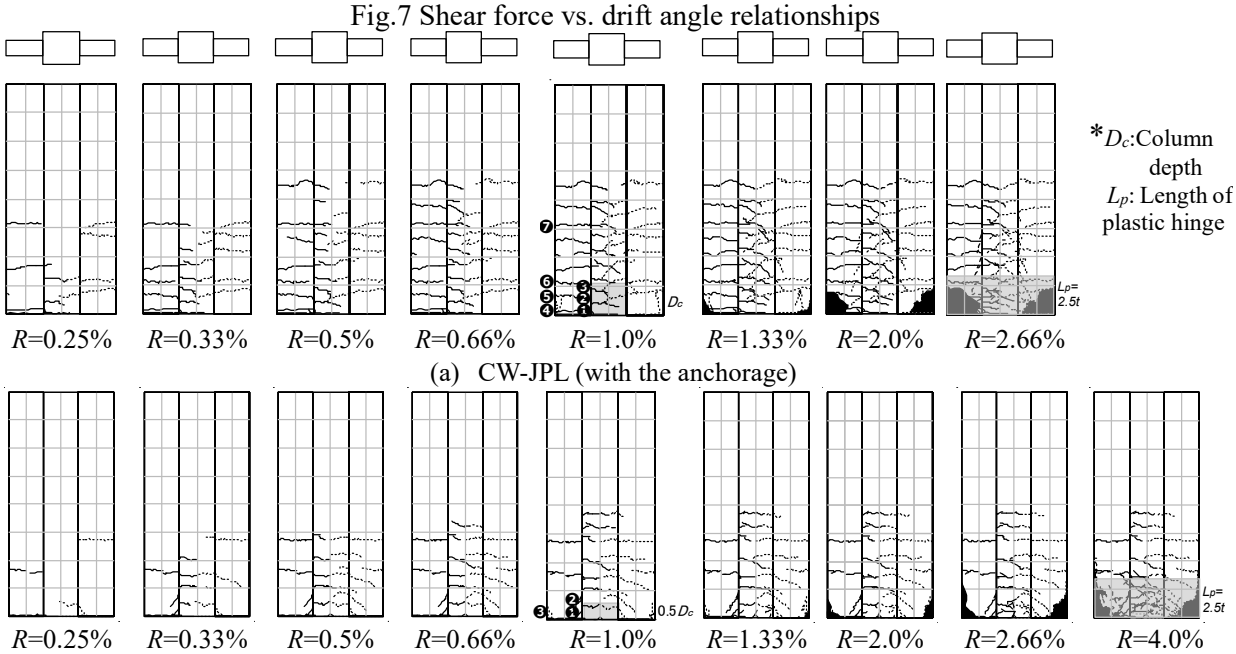

(a) CW-JPL (with the anchorage)

(b) CWN-JPL (without the anchorage)

Fig.8 Damage development of the specimens

the cycle of R = 0.25% rad. In the case of CWN-JPL, only the existing flexural cracks at the bottom of wing walls extended. The column main rebar yielded at the cycle of R = 0.5% rad. then the stiffness significantly degraded in the following cycle. Compressive yielding of the vertical rebar in the wing walls occurred at the cycle of R=1.0% rad. The maximum strengths reached 170.2 kN and -176.3 kN at the peak drifts of the cycles of R=1.0% rad and R = -2.0% rad, respectively. From the following cycle, the lateral load decreased gradually with damage to the wall confined area showing concrete crush at the bottom of the wing wall in a height approximately 2.5 times the wall thickness (shown as Fig. 8(b). The buckling of vertical rebar in the wing walls was observed at the cycle of R = 2.66% rad. The lateral load decreased to 80% of the maximum strength at R = 3.53% rad, and the loading was completed at the cycle of R = 4.0% rad.

3.2 Damage evaluations

The observed damage on the specimens with wing walls was investigated in terms of crack width and length. Crack widths were measured by using an imprinted crack scale card with 0.05 mm intervals. The crack width measurement was conducted at the peak drift and unloading during the first loading cycle with each amplitude. In this study, the crack width was represented by 0.00 mm forvisible cracks with width of less than 0.05 mm. The variation of residual crack lengths and the maximum residual crack widths of the wing walls and column

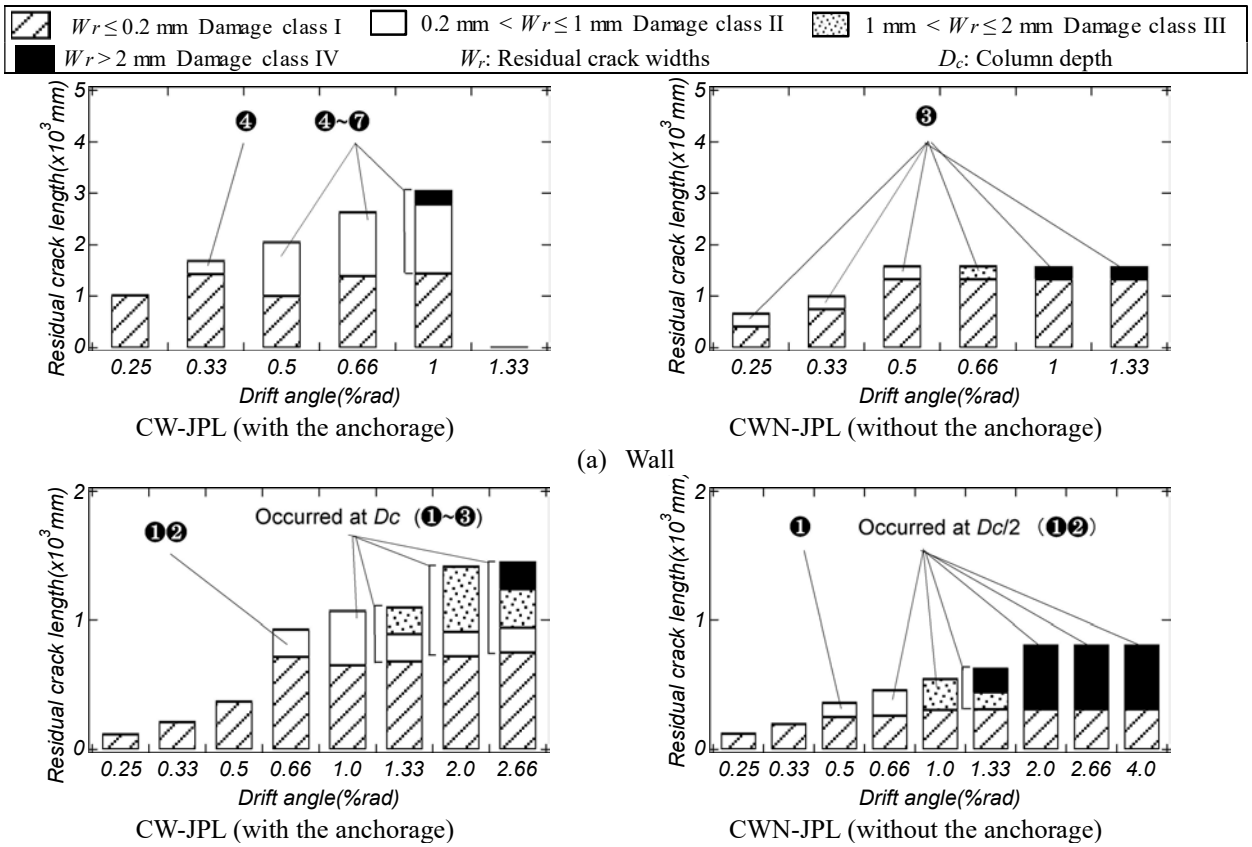

CW-JPL (with the anchorage) CWN-JPL (without the anchorage)

(a) Wall

CW-JPL (with the anchorage) CWN-JPL (without the anchorage)

(b) Column

Fig.9 Transition of total residual crack lengths

after the first loading cycle with each amplitude are shown in Fig. 9 and Fig. 10, respectively. However, in the case of CW-JPL, it was impossible to measure the crack width at the wing wall bottom from the cycle of R=1.0% rad because of remarkable concrete spalling at the wing wall edge. On the other hand, since the concrete spalled out at the wing wall bottom edge of CWN-JPL became remarkable after the cycle of R=1.33% rad, the crack width at the wing wall edge could not be measured. Thus, Fig. 9 (a) shows the transition of total residual crack lengths for CW-JPL/CWN-JPL up to the cycle of R=1.0% rad/1.33% rad. The total crack lengths were evaluated as an indicator to compare the residual crack density on both specimens. The residual cracks were classified based on the widths at unloading, W_r which was categrized as $W_r \leq 0.2$ mm (Damage class I: continuous usage), 0.2 mm < $W_r \leq 1.0$ mm (Damage class II: easily repaired), 1.0mm < $W_r \leq$ 2.0 mm (Damage class III: reparable), W_r >0.2 mm (Damage class IV: stable maintenance of stress due to vertical load after earthquake) referring to the relations of the limit states and damage levels in the AIJ guidelines [3], as shown in Table 7, and their lengths were summed to obtain the total length with each classification.

[Specimen CW-JPL with the wall vertical rebar anchorage]

The total lengths of residual cracks on the walls increased with the occurence/extension of bending cracks on the walls from the cycle of R = 0.25% rad to the cycle of R = 1.0% rad, as shown in Figs. 8(a) and 9(a). The residual crack width on the wing wall (Fig. 8(a) ❹) exceeded 0.2 mm at the cycle of R=0.33% rad after yielding of the wall vertical rebar. A wider range of residual cracks ❺ to ❼ on the wall widened beyond 0.2 mm from the subsequent cycle of R = 0.5% rad. In addition, since the cracks on the wing walls extended onto the column, the cracks were widely distributed over the lower half of the column, as shown in Fig. 8(b). After the cycle of R = 0.66% rad, the residual cracks ❶ and ❷ within the range of D_c from the column bottom widened beyond 0.2 mm, and residual cracks ❸ exceeded 0.2 mm from the R = 1.0% rad.

[Specimen CWN-JPL without the wall vertical rebar anchorage]

The total residual crack lengths on the walls moderately increased with the occurence/extension of bending cracks on the wall from the cycle of R = 0.25% rad to the cycle of R = 0.5% rad, as shown in Fig. 8(b) and

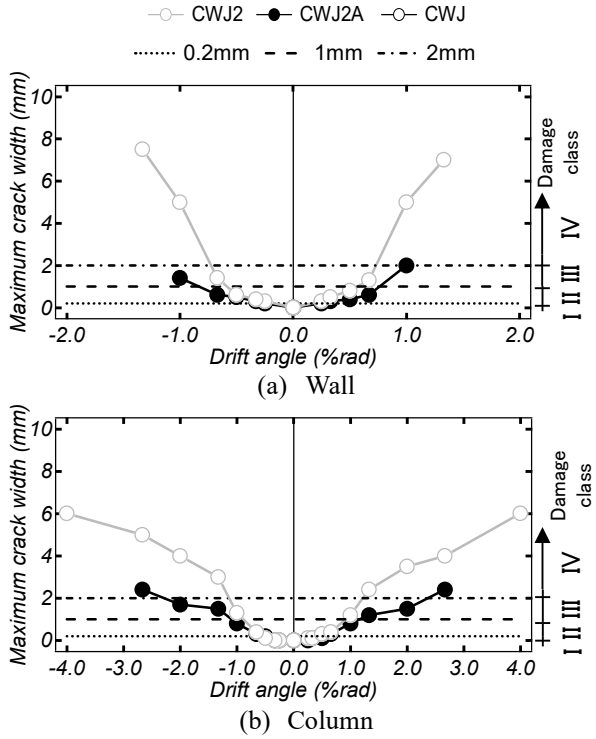

Fig.10 Maximum residual crack widths

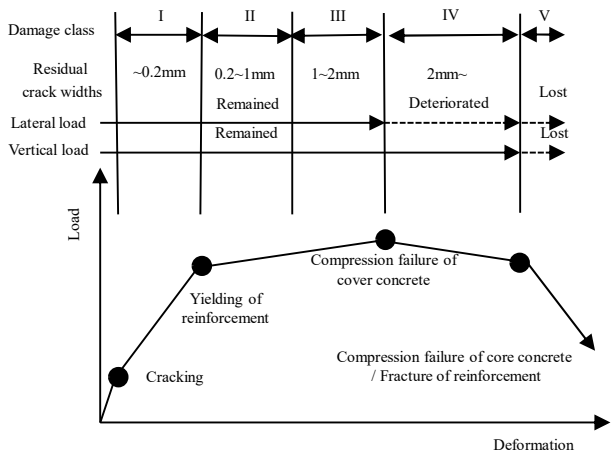

Fig.11 Damage class vs. load carrying capacity (ductile reinforced concrete member) [3]

Table 7 Limit states and corresponding damage class in AIJ guidelines [3]

Limit state	Member state	Damage class	Damage condition		
			Rebar	Concrete	Residual crack widths (W_r)
	Continuous usage	I	Elastic	Nearly elastic	$W_r \leq 0.2$ mm
Serviceability →					
	Easily repaired	II	Yielding of a few	Healthy	0.2 mm< W_r ≤1.0 mm
Repairability I→					
	Reparable	III	No buckling	Healthy (Core concrete)	1.0 mm< W_r ≤2.0 mm
Repairability II→					
	Stable maintenance of stress due to vertical load at the end of the earthquake	IV	No fracture	Compression failure (Cover concrete)	2mm < W_r
Safety →					
	Lateral load capacity degrades	V	Fracture	Compression failure (Core concrete)	

9(a). In the subsequent cycles, since the vertical wall rebar had no anchorage into the base stub, damage to the wall surface was limited, and the total lengths of residual cracks on the wing wall remained almost constant. In the case of CWN-JPL, only the crack ❸ occurred at the boundary between the wall bottom and the stub exceeded 0.2 mm from the cycle of R = 0.25% rad, but the other cracks on the walls were less than 0.2 mm, as shown in Fig. 9(a). Then, the residual crack ❶ within the range of 1/2 of D_c from the column base widened beyond 0.2 mm after the cycle of R = 0.5% rad, and the residual crack ❷ exceeded 0.2 mm from the cycle of R = 0.66% rad. The other residual cracks in the column were less than 0.2 mm.

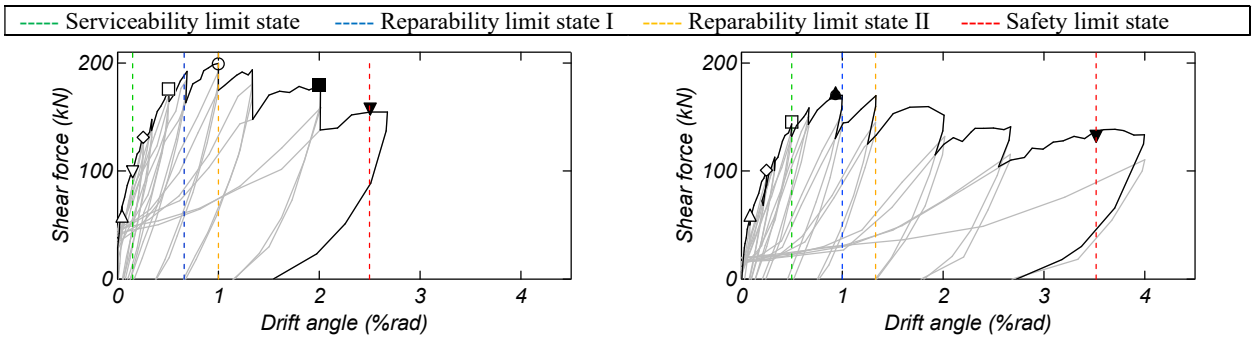

(a) CW-JPL (with Anchorage) (b) CWN-JPL (without Anchorage)

Fig. 12 Shear force – drift angel relationships with damage classes

Table 8 Seismic capacities at the limit states

Specimen	Serviceability		Reparability I		Reparability II		Safety	
	Drift	Shear force	Drift	Shear force	Drift angle	Shear force	Drift angle	Shear force
CW-JPL	0.16%	101 kN	0.66	192 kN	1.0%	199 kN	2.55%	159 kN
CWN-JPL	0.5%	143 kN	1.0	170 kN	1.33%	169 kN	3.53%	136 kN

3.3 Evaluation of the limit states and damage levels

The initial stiffness and maximum strength of the column with the wing walls was significantly higher compared to the column referring to the previous research [7] , demonstrating the possibility that the wing wall could be actively used as an element contributing to structural performance. However, there is no sufficient experimental data on the relationships between the serviceability limit states (the limit forcontinuous usage without repair), reparability limit (the limit for continuous usage after repairing), and safety limit state (the limit of stable maintenance of stress due to vertical load after earthquake) and damage classes for RC columns with wing walls. Therefore, in this study, since both specimens were of the flexure-dominant type, the above-mentioned limit performance of each specimen was determined based on Fig. 10, 11 and Table 7 [3]. However, in determining the safety limit, a reduction point to 80% of the maximum strength (hereafter $0.8Q_{max}$) was applied based on the AIJ standards [4]. In addition, in the structural system proposed in this study (without the wall vertical rebar anchorage), exposure of the wall vertical rebar is limited even after the residual cracks at the wall bottom widen (or the rebar arrangement without exposing them can be adopted). Therefore, the residual cracks at the wing wall bottom of CWN-JPL were not considered in the damage evaluation. Accordingly, the damage on the column was the main factor in determining the damage classes and the limit states for CWN-JPL. Figure 12 shows the damage classes defined under the above assumptions on the envelope of the shear force-drift angle relationships from Fig.7. Since the specimens were symmetrical and the damage to the walls and column in the positive and negative loading was similar, the figure shows the relationships in the loading direction showing the safety limit. Table 8 summarizes the evaluation results of the seismic limit performance.

[Specimen CW-JPL with the wall vetical rabar anchorage]
The wall residual crack width was less than 0.2 mm (damage class I) until the cycle of R = 0.25% rad. However, the serviceability limit state was reached at R = 0.16% rad due to tensile yielding of the wall vertical rebar. The reparability limit state I was reached at R = 0.66% rad because the wall residual crack width attained 0.2~1.0 mm (damage class II) during the cycle of R = 0.33% to R = 0.66% rad. The reparability limit state II was reached at R = 1.0% rad because the wall residual crack width was 1.0~2.0 mm (damage class III) during the cycle of R = 0.66% to R = 1.0% rad. The wall residual crack width was beyond 2.0 mm (damage class IV) during the cycle of R = 1.0% rad. The safety limit state was reached at R = 2.55% since the lateral load decreased to $0.8Q_{max}$.

[Specimen CWN-JPL without the wall vertical rebar anchorage]
The serviceability limit state was reached at R = 0.5% rad due to tensile yielding of the longitudinal rebar at the column base. The reparability limit state I was reached at R = 1.0% rad because the column residual crack

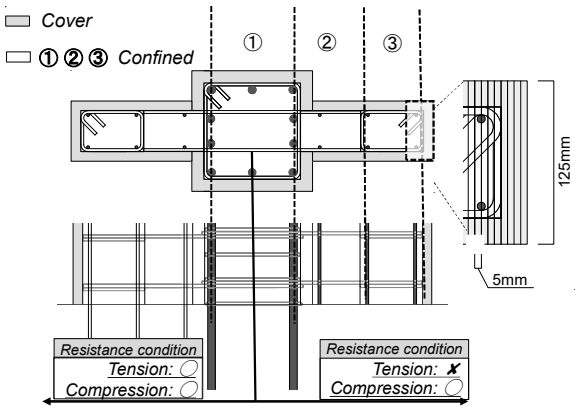

CW-JPL CWN-JPL

Fig.13 Fiber modeling for bending analysis

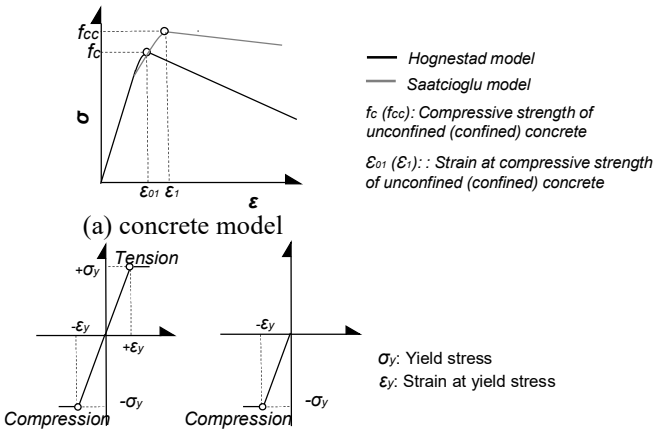

CW-JPL CWN-JPL

(b) steel reinforcement model

Fig.14 Constitutive laws for concrete / reinforcement

width was 0.2~1.0 mm (damage class II) during the cycle of R = 0.5% to R = 1.0% rad. The column residual crack width was 2.0 mm (damage class III) and exceeded 2 mm (damage class IV) at the cycle of R = 1.0% and 1.33% rad, respectively; thus, the reparability limit state II was evaluated at R = 1.3% rad. The safety limit state was reached at R = 3.53% rad since the lateral load decreased to $0.8Q_{max}$.

Focusing on the effects of the anchorage of the wall vertical rebar, the drifts at the serviceability limit state, the reparability limit state I, and reparability limit state II of CWN-JPL without the anchorage were 3.1, 1.5 and 1.3 times those of CW-JPL with the anchorage. In particular, by eliminating theanchorage, tensile yielding of the vertical rebar at the wall bottom were prevented. As a result, the drift at the serviceability limit state corresponding to the tensile yielding of the column logitudinal rebar wassignificantly increased; thus, the shear force that can be borne at the serviceability limit was greatly improved (see Table 8). This result is nothing but the realization of the original aim of proposing this structure that eliminates the anchorage of the wall vertical rebar. In terms of the safety limits, the drift capacity of CWN-JPL was 1.4 times that of the CW-JPL. This is also because of eliminating the anchorage of the vertical wall rebars, namely tensile yielding of the wall vertical rebars was avoided; thus, the integrity with the surrounding concrete was maintained until the larger deformation.

4. Numerical simulation of the experimental performance of the specimens

4.1 Bending analysis

From the experimental results in Section 3.1, both the specimens were of the flexure-dominant type; thus, bending analysis was performed based on the fiber model. The bending analysis assumed Navier's hypothesis for the cross sections which were replaced by concrete elements with a depth of 5 mm and steel elements, as shown in Fig. 13. For concrete, the cover and confined areas were distinguished, as shown in the figure. However, since the CWN-JPL removed the anchorage of the wall vertical rebar, the resistance to tensile stress of the wall vertical rebar was neglected. On the other hand, since the wall vertical rebar of the specimen yielded in compression in the experiment, they were assumed to resist compression. As for the axial force in the bending analysis, a constant axial force 162kN was applied to the cross section of column as in the experiment. The Hognestad model [8] (black line) and Saatcioglu model [9] (gray line) were adopted for the envelope compressive stress-strain relationships of cover and core concrete, respectively, as shown in Fig. 14 (a), while tensile stress resistance was neglected for the concrete. The stress-strain relationship of each concrete model is given by Eqs.3 and 4.

〈Hognestad model〉

$$\sigma(\varepsilon_x) = f_c\left[\frac{2\varepsilon_x}{\varepsilon_{01}} - \left(\frac{\varepsilon_x}{\varepsilon_{01}}\right)^2\right] \qquad 0 \le \varepsilon_x < \varepsilon_{01}$$

$$\sigma(\varepsilon_x) = \frac{3f_c\varepsilon_x + f_c(17\varepsilon_{01} - 20\varepsilon_{085})}{20(\varepsilon_{01} - \varepsilon_{085})} \qquad \varepsilon_{01} < \varepsilon_x \tag{3}$$

〈Saatcioglu model〉

$$\sigma(\varepsilon_x) = f_{cc}\left[\frac{2\varepsilon_x}{\varepsilon_1} - \left(\frac{\varepsilon_x}{\varepsilon_1}\right)^2\right]^{1/(1+2K)} \qquad 0 \le \varepsilon_x < \varepsilon_1$$
$$\sigma(\varepsilon_x) = \frac{3f_{cc}\varepsilon_x + f_c(17\varepsilon_1 - 20\varepsilon_{85})}{20(\varepsilon_1 - \varepsilon_{85})} \qquad \varepsilon_1 < \varepsilon_x \tag{4}$$

where f_c (f_{cc}): compressive strength of unconfined (confined) concrete, ε_{01} (ε_1): strain at compressive strength of (confined) concrete, ε_{085} (ε_{85}): strain at 85% compressive strength of unconfined (confined) concrete, K: coefficient considering confining effect (CW-JPL: ① / ② / ③ = 0.184 / 0.068 / 0.082, CWN-JPL: ① / ② / ③ = 0.167 / 0.063 / 0.075).

A bi-linear model was used for the stress-strain relationship of reinforcement, as shown in Fig. 14 (b). The mechanical properties of concrete and the reinforcement were referred from the experimental results, as shown in Tables 3 and 4.

4.2 Analysis results

The shear force-drift angle relationships obtained from the bending analysis are shown in Fig. 7 with the solid red line to compare with the experimental results. The drift angle R was combined the deformation component at flexural yielding R_y at the yielding of tensile edge rebar and the plastic deformation component R_p after that, and the relationship between the curvature φ and the drift angle R is given by Eq. 5.

$$R = R_y + R_p$$
$$R_y = \frac{\Delta_y}{L} = \frac{\varphi_y \cdot L}{3} \tag{5}$$
$$R_p = \frac{\Delta_p}{L} = \frac{\varphi_p \cdot L_p \cdot (L - L_p/2)}{L}$$

where Δ_y: deformation at yielding of the tensile edge rebar, φ_y: curvature at yielding of the tensile edge rebar, L: inflection point height (= 1600 mm), L_p: height of plastic hinge, Δ_p: plastic deformation after yielding of the tensile edge rebar, φ_p: plastic curvature after yielding of the tensile edge rebar. The height L_p of the plastic hinge on the compression side was evaluated to be 312.5 mm, which was 2.5 times the wall thickness t, based on the experimental results as shown in Fig. 8.

The experimental results could be evaluated accurately from the analysis results up to the maximum strength for both the specimens based on Fig. 4. The post-peak envelop curves from the experiment of both the specimens also agreed well with the simulation results. Therefore, the seismic performance of both specimens could be estimated with good accuracy by the presented method.

5. Conclusions

This study proposed a new rebar arrangement of wing walls which removed the wall vertical rebar anchorage to reduce earthquake damage. A series of static cyclic loading tests was performed to study the effects of the removal of wall vertical rebar anchorage on their seismic performance. Furthermore, conventional bending analysis was carried out to simulate the seismic performance of the specimens. The major findings of this study are summarized below.

1) Comparing both specimens with and without the wall vertical rebar anchorage, the initial stiffness and maximum strength of the conventional specimen CW-JPL was relatively higher because of the presence of anchorage, while the deformation capacity of CWN-JPL was higher by the absence of anchorage. The anchorage removal reduced concrete damage caused by the wall vertical rebar, which could delay

compression failure of concrete in the confined zone of the wall.

2) In the structural system proposed in this study, the residual cracks at the boundary between the wall bottom and the base stab were relatively large due to the absence of anchorage, however, which is not likely to affect the structural durability/safety considering the facts that the exposure of the vertical rebar at the wall bottom is limited, or that some arrangement without exposing the vertical rebar can be adopted. Therefore, the serviceability limit of the test piece was examined with the presence or absence of wall vertical rebar anchorage as a variable and without considering the residual cracks in the wall bottom boundary. As a result, the serviceability limit of CWN-JPL without the anchorage allowed higher deformation capacity 3.1 times that of CW-JPL with the anchorage. As for the reparability I, II and the safety limit, CWN-JPL also allowed higher deformation capacities 1.5, 1.3 and 1.4 times those of CW-JPL, respectively.

3) From the experimental results, it was confirmed that each specimen crushed at the bottom of the wing wall in a height approximately 2.5 times the wall thickness on the wall edge after flexural yielding. Since the mechanism type of both the specimens was the flexural-dominant one, the bending behavior of each specimen was simulated using conventional bending analysis. Consequently, the simulation results agreed well with the experimental results showing the reliability of the analysis model.

6. Acknowledgements

This study was supported by a part of the 2018 Tokyo Metropolitan Resilience Project. The authors also would like to acknowledge that the support of former students Misako Tsubaki and Yuki Momoka of Osaka university.

7. References

[1] Architectural Institute of Japan (2012): Preliminary Reconnaissance Report of the 2011 Tohoku-Chiho Taiheiyo-Oki Earthquake.

[2] Architectural Institute of Japan (2017): Survey research report on seismic performance of educational facilities (in Japanese).

[3] Architectural Institute of Japan (2004): Guidelines for Performance Evaluation of Earthquake Resistant Reinforced Concrete Buildings (in Japanese).

[4] Architectural Institute of Japan (2021): AIJ Standard for Lateral Load-carrying Capacity Calculation of Reinforced Concrete Structures (in Japanese).

[5] American Concrete Institute (2019): Building Code Requirements for Structural Concrete (ACI 318-19) and Commentary (ACI318R-19).

[6] Architectural Institute of Japan (2018): AIJ Standard for Structural Calculation of Reinforced Concrete Structures revised 2018 (in Japanese).

[7] Tsubaki, M., Sanada, Y., Zhang, Z., Kusunoki, K., Hibino, Y. and Mukai, T (2019): Experimental Structural Performance Evaluation of RC Columns with Wing Walls without Wall Vertical Rebar Anchorage (in Japanese), *Journal of Structural and Construction Engineering (Transactions of AIJ)*, Vol.84, No.762, pp.1093-1102.

[8] Hognestad E., Hanson N.W., and McHenry D. (1955): Concrete Stress Distribution in Ultimate Strength Design, *ACI Journal*, 52(12): 455-480.

[9] Saatcioglu, M. and Razvi, S. R. (1992): Strength and Ductility of Confined Concrete, *Journal of Structural Engineering*, ACSE, V. 118, No. 6, pp. 1590-1607.

